Supplementary data

Adsorption kinetics and solubilisation of ciprofloxacin in quaternary ammonium based surface active compounds: Experimental and computational study

Ab Raouf Bhat and Rajan Patel*

Biophysical Chemistry Laboratory, Centre for Interdisciplinary Research in Basic Sciences, Jamia Millia Islamia, New Delhi, India.

*Corresponding author.

Tel.: +91 8860634100; fax: +91 11 26983409.

Email address: rpatel@jmi.ac.in, (Dr. R. Patel)

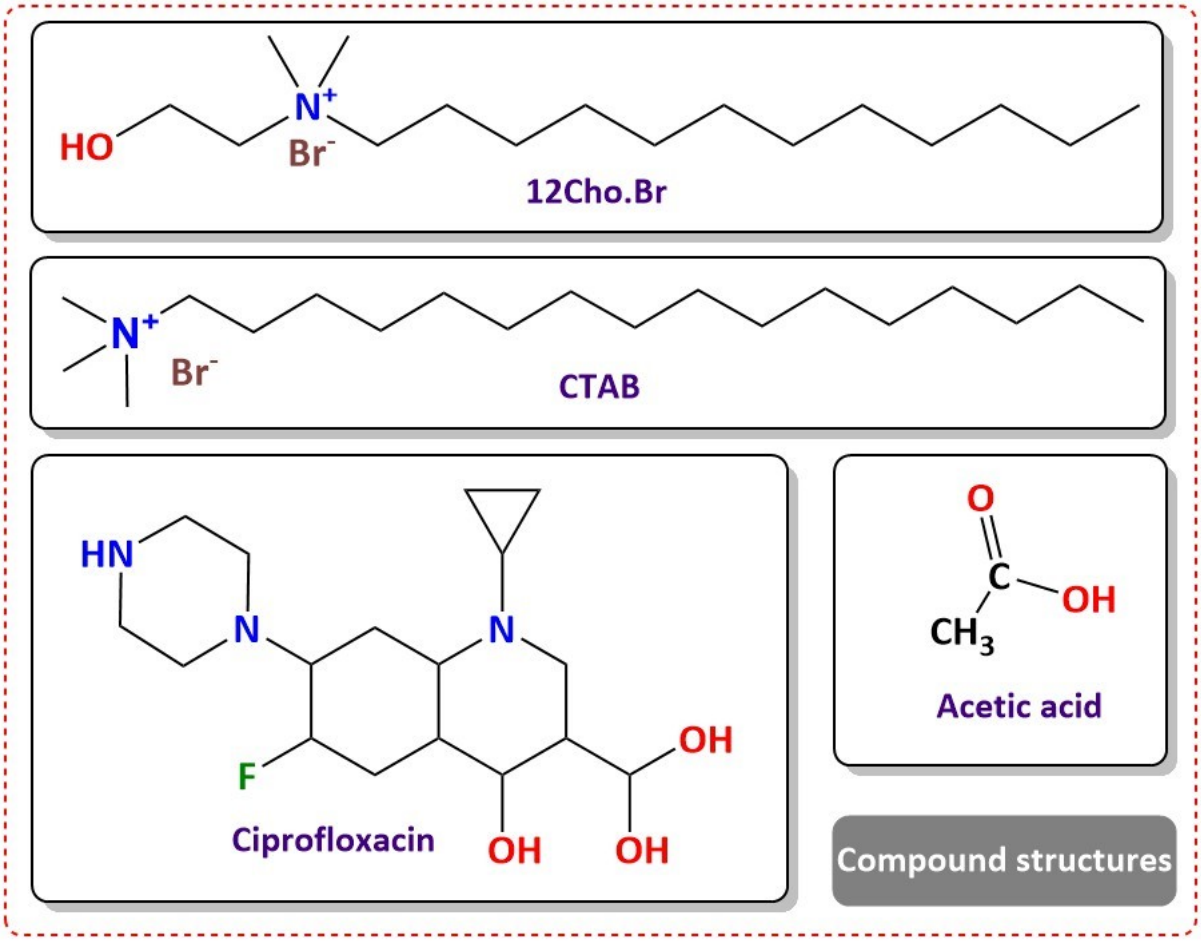

Scheme S1. Showing the 2D structure of compounds used in the study.

Figure captions:

Figure S1. Generalized dynamic interfacial tension, γ_t versus log time (s), curve--region I: induction; region II: rapid fall; region III: meso-equilibrium; region IV: equilibrium.

Figure S2 (a-d). DIFT versus surface age (s) for 12Cho.Br (a), 12Cho.Br(0.3%Ac) (b), 12Cho.Br-CIP (c) and 12Cho.Br-CIP(0.3%Ac) (d), in aqueous medium at different concentration at 298.15K.

Figure S3 (a-d). DIFT versus surface age (s) for CTAB (a), CTAB(0.3%Ac) (b), CTAB-CIP (c) and CTAB-CIP(0.3%Ac) (d) in aqueous medium at different concentration at 298.15K.

Figure S4. DIFT profiles of 0.3% acetic acid, 30μM CIP and 30μM CIP in presence 0.3% acetic acid in aqueous medium as a function of time(s).

Figure 5 (a-c). DIFT as a function of t1/2 (a), t−1/2 (b) and plot of log(γo-γt/γt-γm) versus logt (c) for 12Cho.Br-CIP (30μM CIP) at different concentration at 298.15K.

Figure S6 (a-c). DIFT as a function of $t^{1/2}$ (a), $t^{-1/2}$ (b) and plot of $log(\gamma_o-\gamma_t/\gamma_t-\gamma_m)$ versus *logt* (c) for 12Cho.Br(0.3%Ac) at different concentration at 298.15K.

Figure S7 (a-c). DIFT as a function of $t^{1/2}$ (a), $t^{-1/2}$ (b) and plot of $log(\gamma_o-\gamma_t/\gamma_t-\gamma_m)$ versus *logt* (c) for 12Cho.Br-CIP (0.3%Ac) at different concentration at 298.15K.

Figure S8 (a-c). DIFT as a function of $t^{1/2}$ (a), $t^{-1/2}$ (b) and plot of $log(\gamma_o-\gamma_t/\gamma_t-\gamma_m)$ versus *logt* (c) for CTAB(0.3%Ac) at different concentration at 298.15K.

Figure S9 (a-c). DIFT as a function of t1/2 (a), t−1/2 (b) and plot of log(γo-γt/γt-γm) versus logt (c) for CTAB-CIP (30μM CIP) at different concentration at 298.15K.

Figure S10 (a-c). DIFT as a function of $t^{1/2}$ (a), $t^{-1/2}$ (b) and plot of $log(\gamma_o-\gamma_t/\gamma_t-\gamma_m)$ versus *logt* (c) for CTAB-CIP (0.3%Ac) at different concentration at 298.15K.

Figure S11 (a-c). DIFT as a function of $t^{1/2}$ (a), $t^{-1/2}$ (b) and plot of $log(\gamma_o-\gamma_t/\gamma_t-\gamma_m)$ versus *logt* (c) for (4mM) 12Cho.Br with different concentration of CIP at 298.15K.

Figure S12 (a-c). DIFT as a function of $t^{1/2}$ (a), $t^{-1/2}$ (b) and plot of $log(\gamma_o-\gamma_t/\gamma_t-\gamma_m)$ versus *logt* (c) for (4mM) 12Cho.Br(0.3%Ac) with different concentration of CIP at 298.15K.

Figure S13 (a-c). DIFT as a function of $t^{1/2}$ (a), $t^{-1/2}$ (b) and plot of $log(\gamma_o-\gamma_t/\gamma_t-\gamma_m)$ versus *logt* (c) for (0.5mM) CTAB with different concentration of CIP at 298.15K.

Figure S14 (a-c). DIFT as a function of $t^{1/2}$ (a), $t^{-1/2}$ (b) and plot of $log(\gamma_o-\gamma_t/\gamma_t-\gamma_m)$ versus *logt* (c) for (0.5mM) CTAB (0.3%Ac) with different concentration of CIP at 298.15K.

Figure S15 (a-d): UV-Visible spectra of CIP at various concentrations solubilized in 12Cho.Br and CTAB systems at 298K.

Figure S16 a-b). Variation of $ln(I_0/I)$ with quencher concentration in aqueous solution at 25 °C.

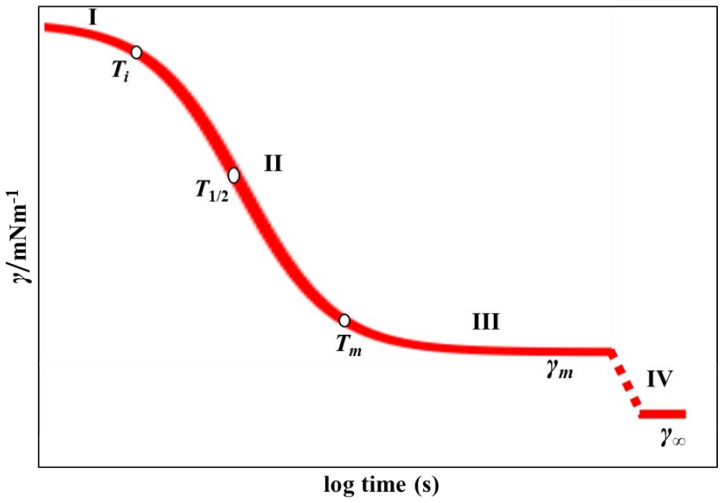

Figure S1. Generalized dynamic interfacial tension, γ_t versus log time (s) curve - region I: induction; region II: rapid fall; region III: meso-equilibrium; region IV: equilibrium.

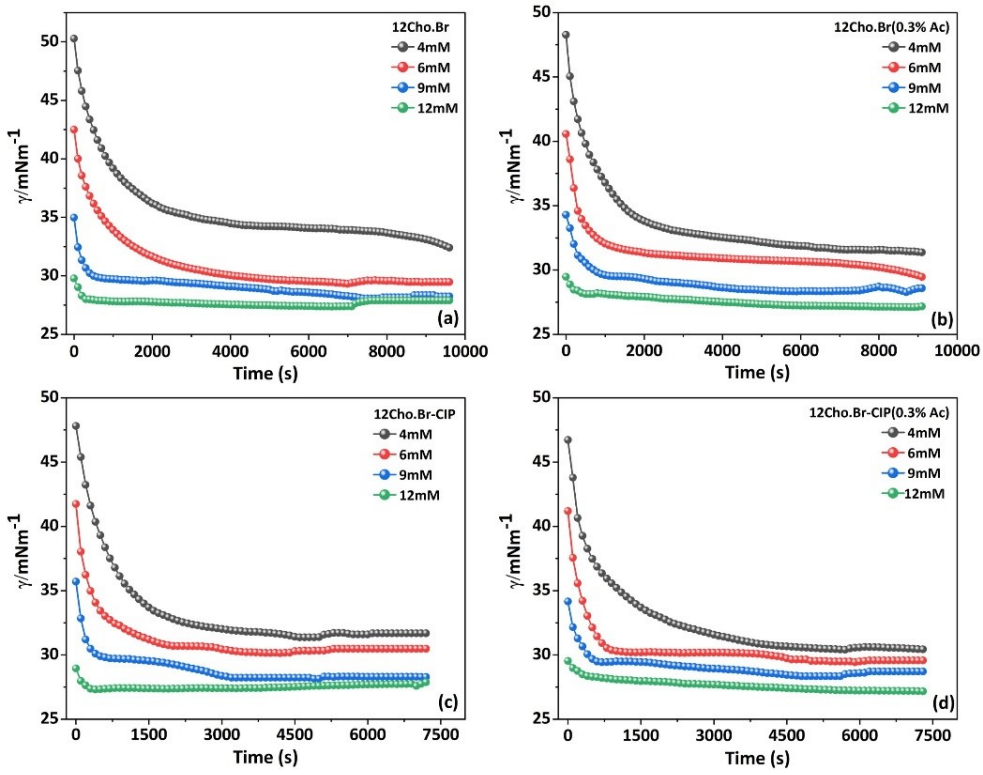

Figure S2 (a-d). DIFT versus surface age (s) for 12Cho.Br (a), 12Cho.Br(0.3%Ac) (b), 12Cho.Br-CIP (c) and 12Cho.Br-CIP(0.3%Ac) (d), in aqueous medium at different concentration at 298.15K.

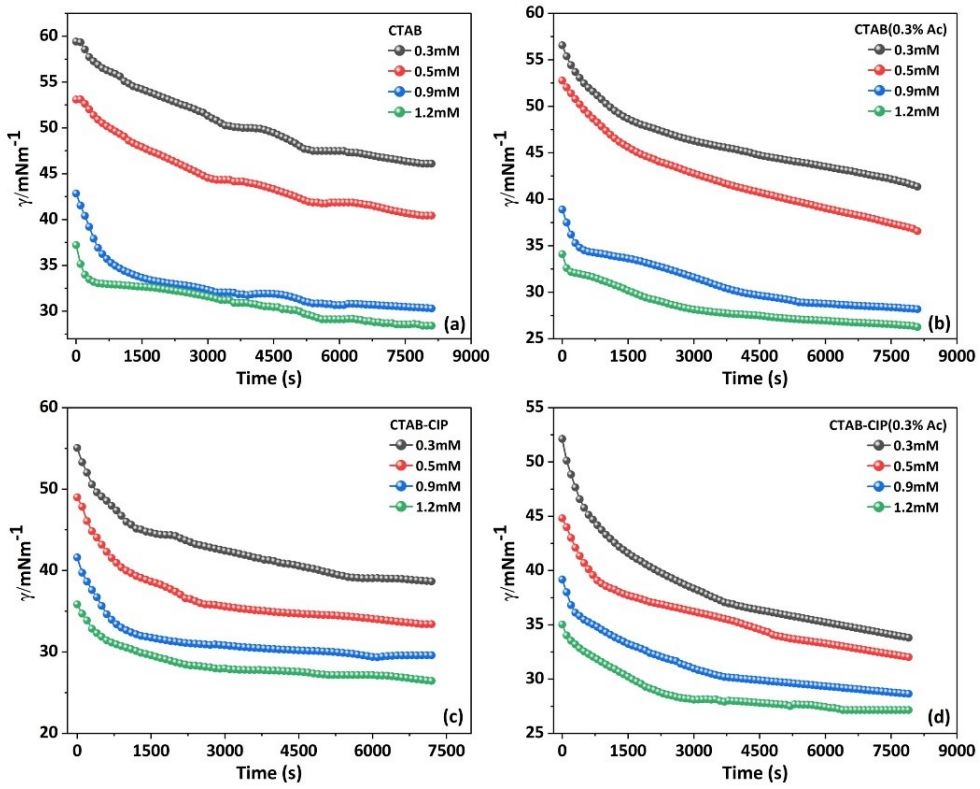

Figure S3 (a-d). DIFT versus surface age (s) for CTAB (a), CTAB(0.3%Ac) (b), CTAB-CIP (c) and CTAB-CIP(0.3%Ac) (d) in aqueous medium at different concentration at 298.15K.

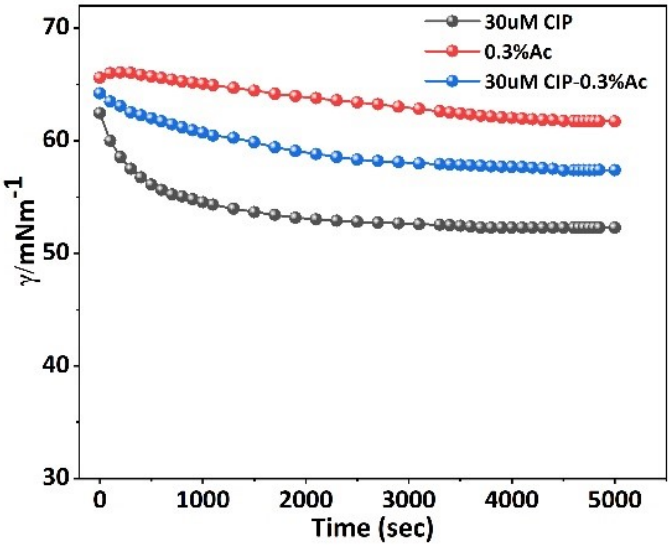

Figure S4. DIFT profiles of 0.3% acetic acid, 30µM CIP and 30µM CIP in presence 0.3% acetic acid in aqueous medium as a function of time(s).

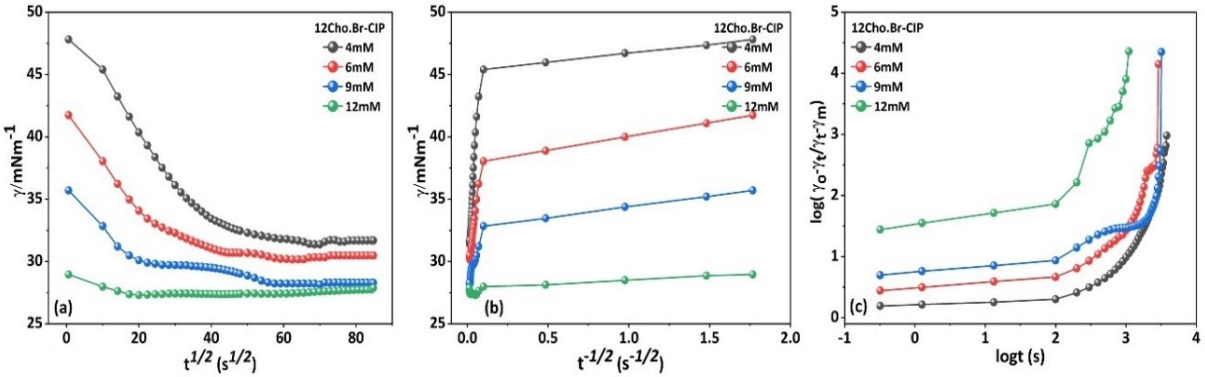

Figure 5 (a-c). DIFT as a function of t1/2 (a), t−1/2 (b) and plot of log(γo-γt/γt-γm) versus logt (c) for 12Cho.Br-CIP (30µM CIP) at different concentration at 298.15K.

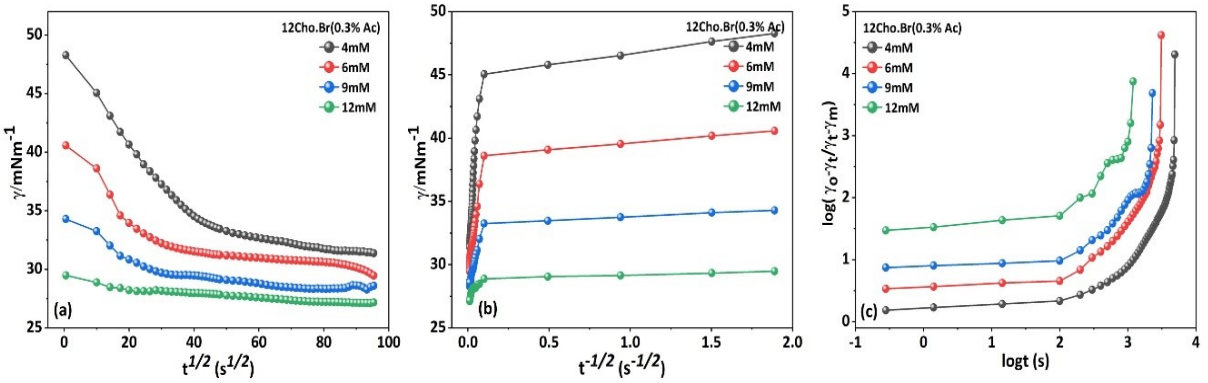

Figure S6 (a-c). DIFT as a function of $t^{1/2}$ (a), $t^{-1/2}$ (b) and plot of $log(\gamma_o-\gamma_t/\gamma_t-\gamma_m)$ versus *logt* (c) for 12Cho.Br(0.3%Ac) at different concentration at 298.15K.

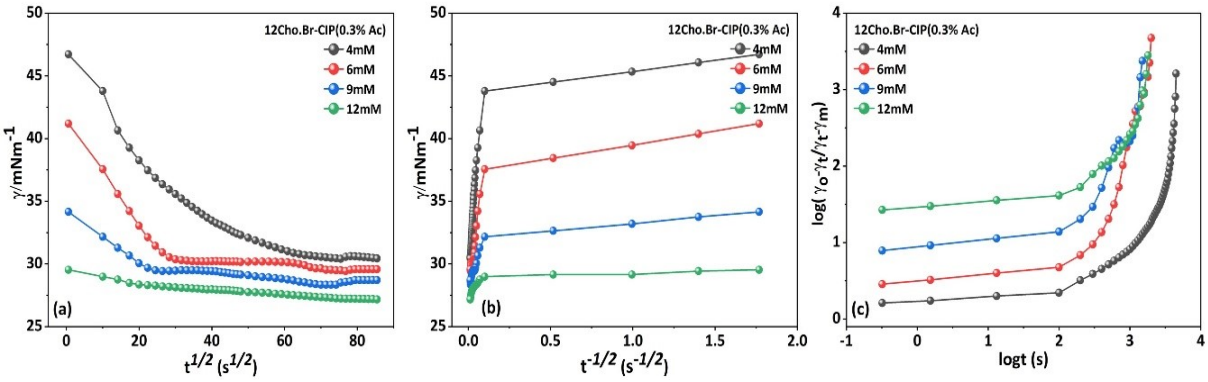

Figure S7 (a-c). DIFT as a function of $t^{1/2}$ (a), $t^{-1/2}$ (b) and plot of $log(\gamma_o-\gamma_t/\gamma_t-\gamma_m)$ versus *logt* (c) for 12Cho.Br-CIP (0.3%Ac) at different concentration at 298.15K.

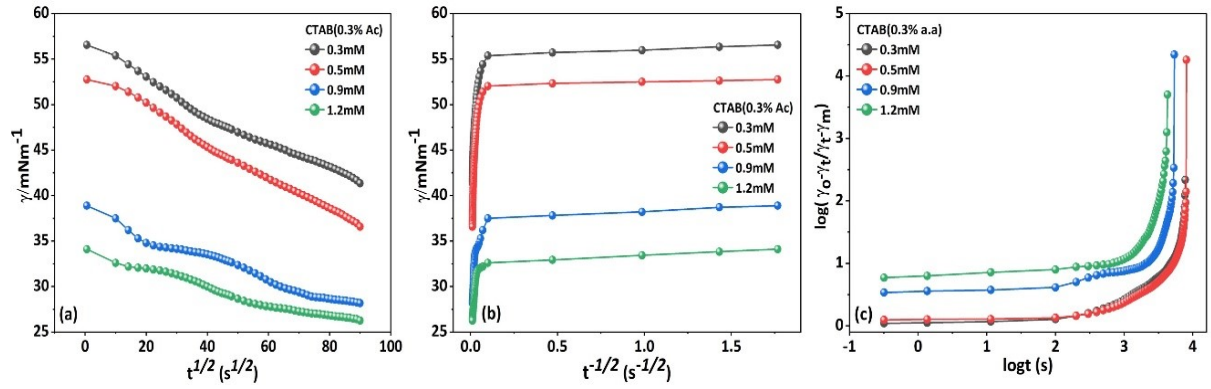

Figure S8 (a-c). DIFT as a function of $t^{1/2}$ (a), $t^{-1/2}$ (b) and plot of $log(\gamma_o-\gamma_t/\gamma_t-\gamma_m)$ versus $logt$ (c) for CTAB(0.3%Ac) at different concentration at 298.15K.

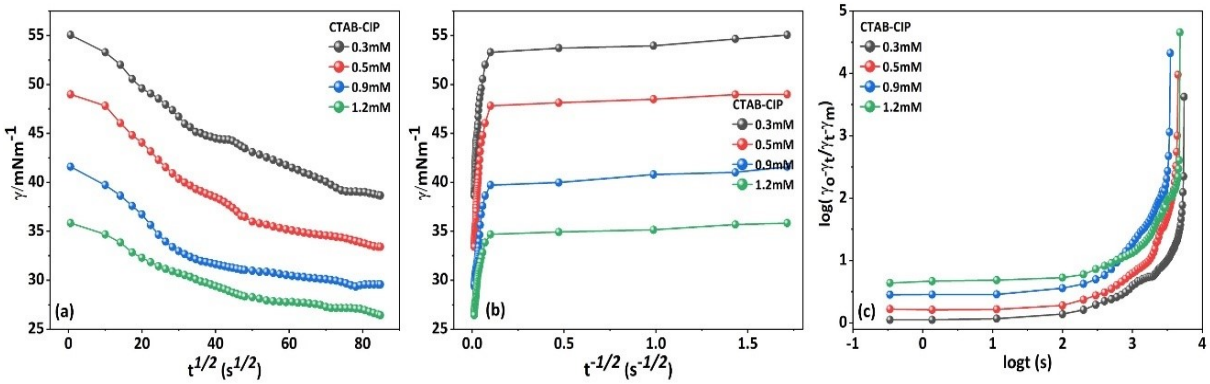

Figure S9 (a-c). DIFT as a function of t1/2 (a), t−1/2 (b) and plot of log(γo-γt/γt-γm) versus logt (c) for CTAB-CIP (30µM CIP) at different concentration at 298.15K.

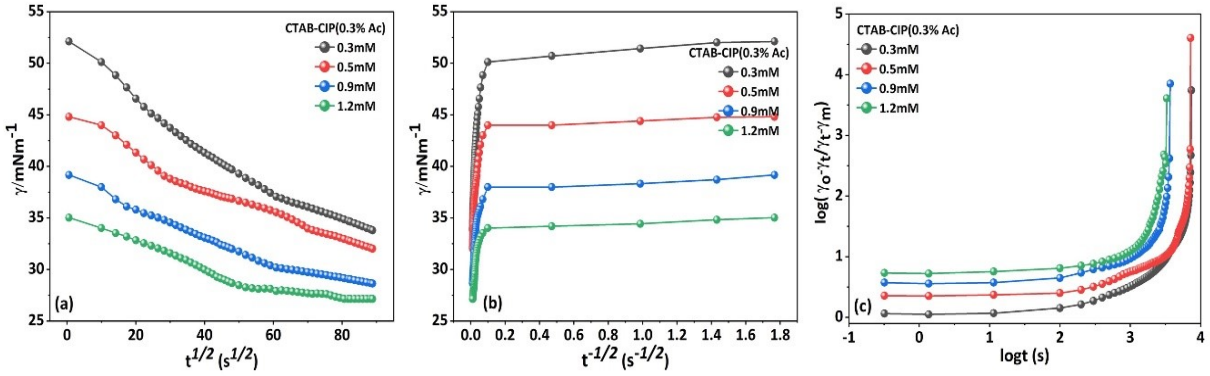

Figure S10 (a-c). DIFT as a function of $t^{1/2}$ (a), $t^{-1/2}$ (b) and plot of $log(\gamma_o-\gamma_t/\gamma_t-\gamma_m)$ versus $logt$ (c) for CTAB-CIP (0.3%Ac) at different concentration at 298.15K.

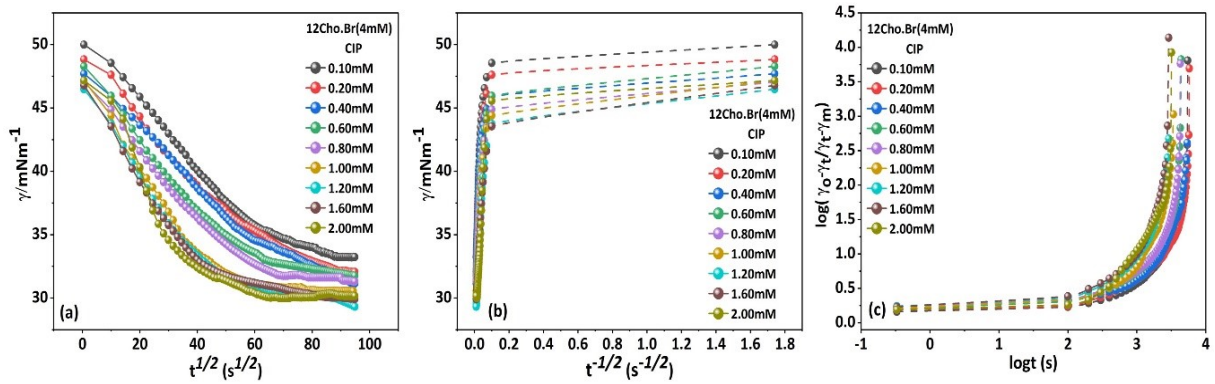

Figure S11 (a-c). DIFT as a function of $t^{1/2}$ (a), $t^{-1/2}$ (b) and plot of $log(\gamma_o-\gamma_t/\gamma_t-\gamma_m)$ versus $logt$ (c) for (4mM) 12Cho.Br with different concentration of CIP at 298.15K.

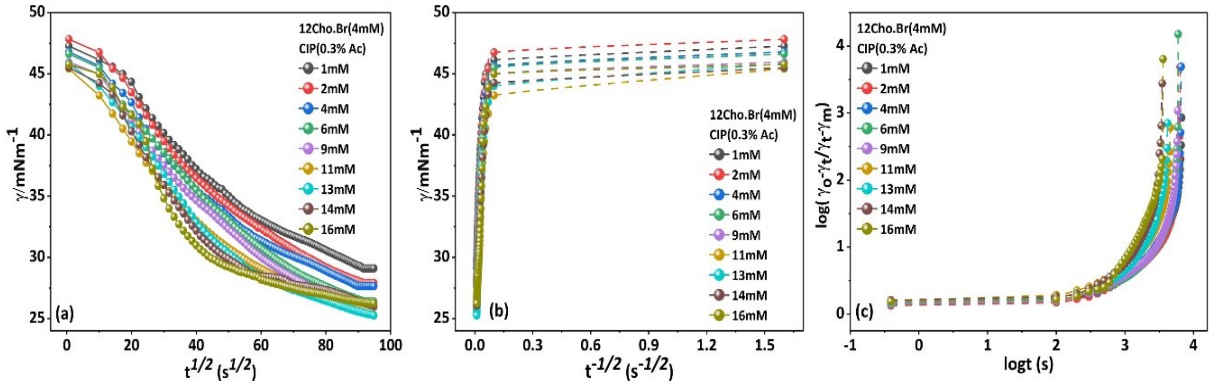

Figure S12 (a-c). DIFT as a function of $t^{1/2}$ (a), $t^{-1/2}$ (b) and plot of $log(\gamma_o-\gamma_t/\gamma_t-\gamma_m)$ versus $logt$ (c) for (4mM) 12Cho.Br(0.3%Ac) with different concentration of CIP at 298.15K.

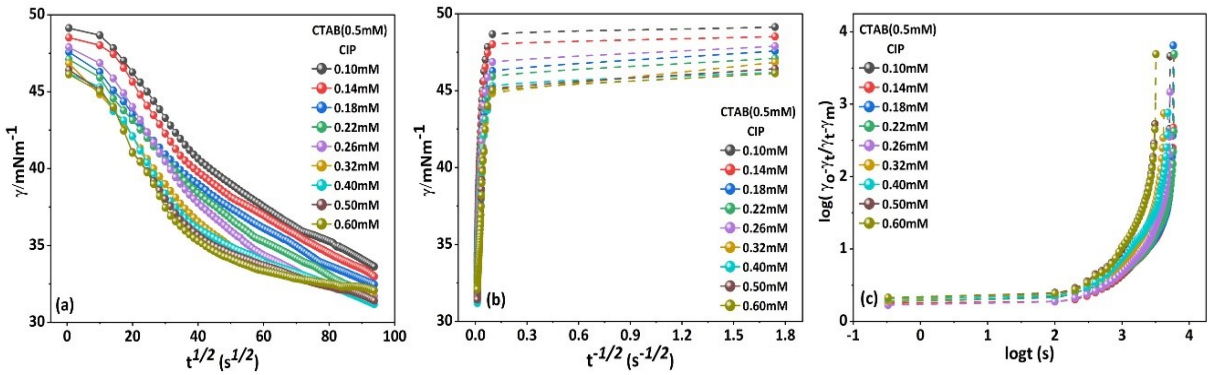

Figure S13 (a-c). DIFT as a function of $t^{1/2}$ (a), $t^{-1/2}$ (b) and plot of $log(\gamma_o-\gamma_t/\gamma_t-\gamma_m)$ versus $logt$ (c) for (0.5mM) CTAB with different concentration of CIP at 298.15K.

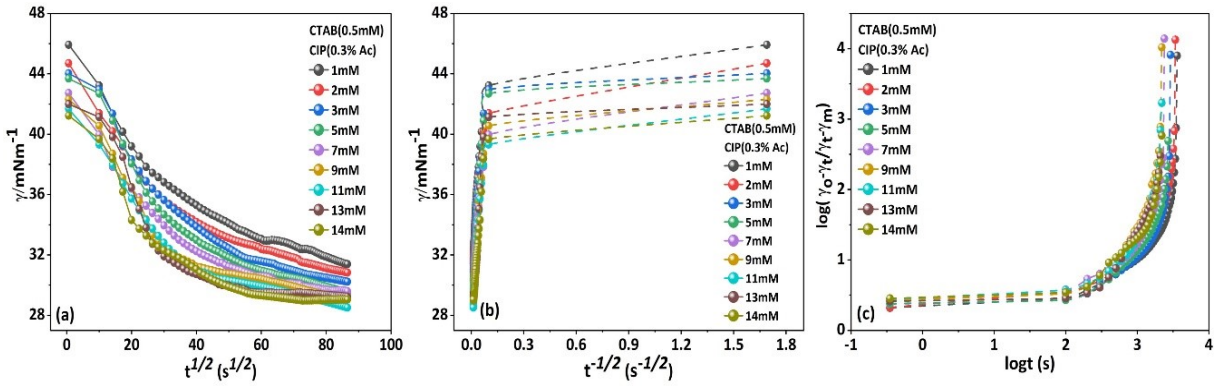

Figure S14 (a-c). DIFT as a function of $t^{1/2}$ (a), $t^{-1/2}$ (b) and plot of $log(\gamma_o-\gamma_t/\gamma_t-\gamma_m)$ versus $logt$ (c) for (0.5mM) CTAB (0.3%Ac) with different concentration of CIP at 298.15K.

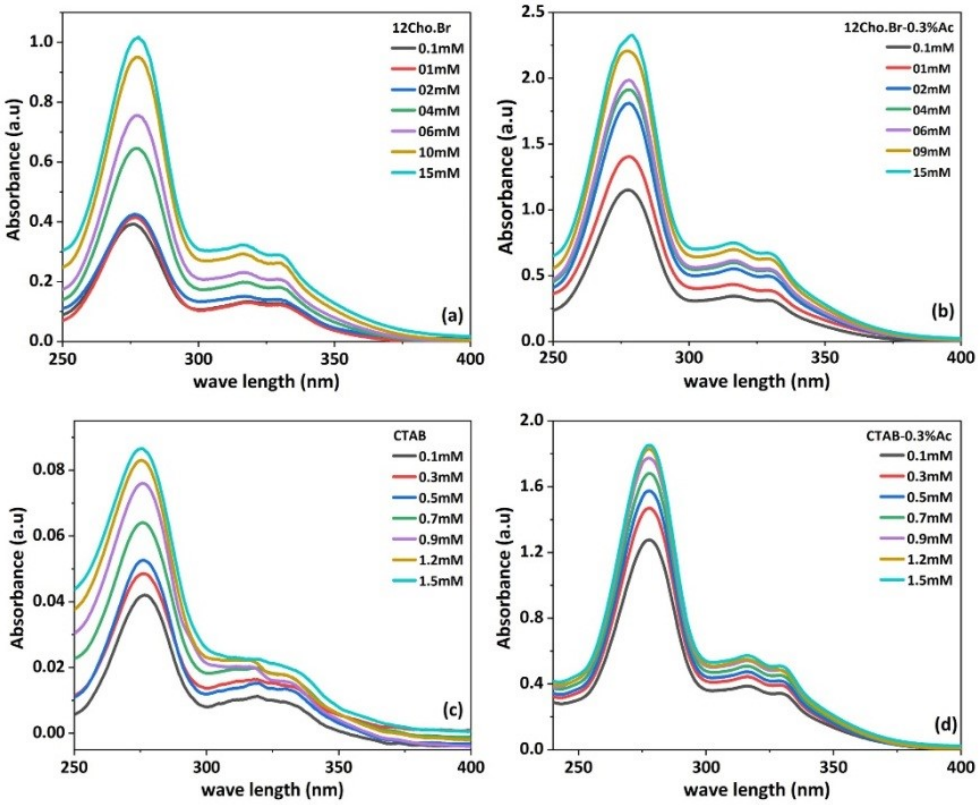

Figure S15 (a-d): UV-Visible spectra of CIP at various concentrations solubilized in 12Cho.Br and CTAB systems at 298K.

Aggregation number

Steady-state fluorescence measurements were carried out using Cary Eclipse fluorescence spectrophotometer, Agilent technology. at temperature 25 ± 0.1 °C. A quartz cuvette of 1 cm path length was used to record the spectra. Pyrene fluorescence probe spectroscopy was utilised to study the aggregation number of the 12Cho.Br and CTAB systems. The emission spectra of pyrene were recorded from 340 to 450 nm using an excitation wavelength of 334 nm. Excitation and emission band slits were kept at 5 nm. The micelles aggregation number (N_{agg}) was concluded by performing a pyrene fluorescence quenching experiment using the quencher cetylpyridinium chloride and the following equation S1 was utilised.

$$ln\ (I_0/I) = N_{agg}C_Q / C_{SACs} - cmc \qquad \text{(S1)}$$

where, I_0 and I are the fluorescence emission intensities of pyrene in the absence and presence quencher. C_{SACs} and C_Q are the concentration of 12Cho.Br and CTAB and quencher respectively. Figure S16 displays the $ln(I_0/I)$ plot for the different SACs systems as a function of quencher concentration.

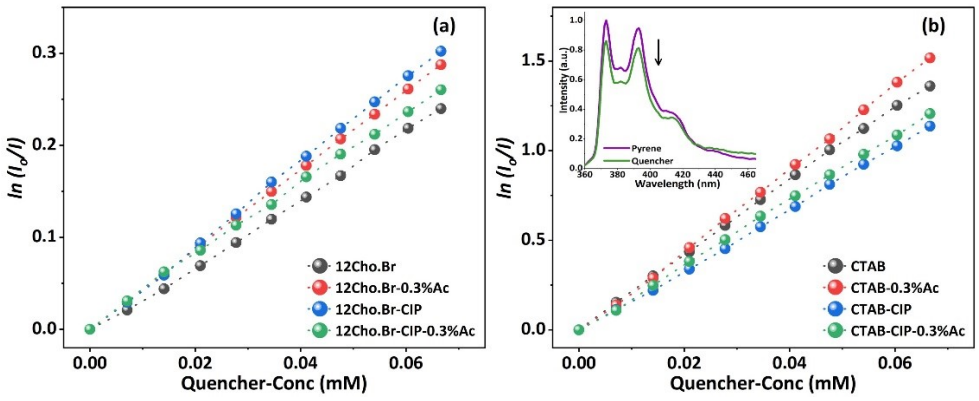

Figure S16 (a-b). Variation of $ln(I_0/I)$ with quencher concentration in aqueous solution at 25 °C.

System	HOMO	LUMO
CIP	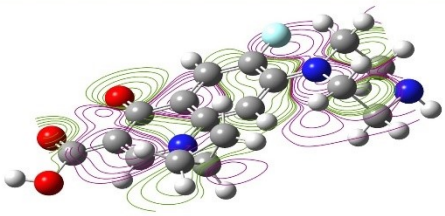	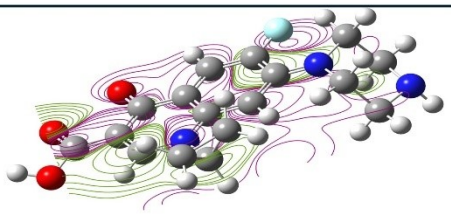
12Cho.Br	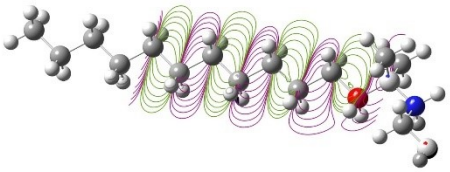	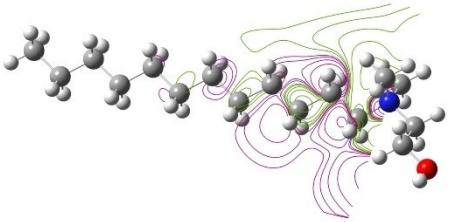
CTAB	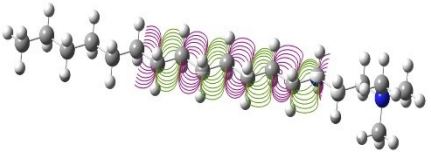	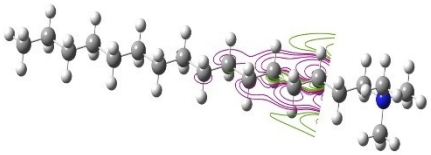

System	HOMO	LUMO
12Cho.Br-CIP	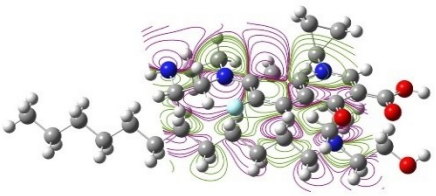	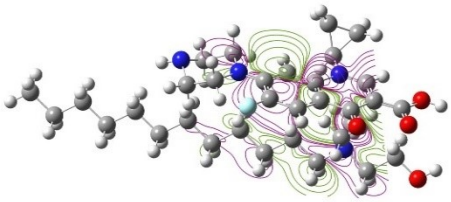
CTAB-CIP	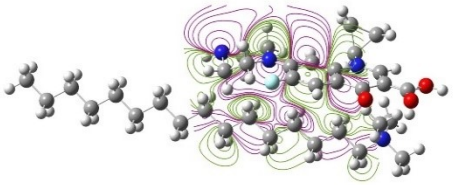	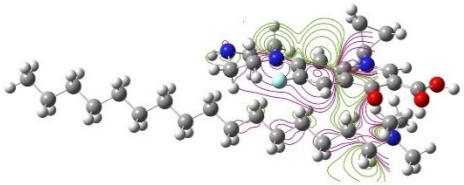

Figure S17 Optimized structures of CIP, 12Cho.Br, CTAB, 12Cho.Br-CIP and CTAB-CIP with corresponding 2D electrostatic potential profiles

Table captions:

Table S1. DIFT parameters for (4mM) 12Cho.Br with different concentration of CIP at 298.15K.

Table S2. DIFT parameters for (4mM) 12Cho.Br(0.3%Ac) with different concentration of CIP at 298.15K.

Table S3. DIFT parameters for (0.5mM) Ctab with different concentration of CIP at 298.15K.

Table S4. DIFT parameters for (0.5mM) CTAB (0.3%Ac) with different concentration of CIP at 298.15K.

Table S5. Showing different parameters calculated from UV-Visible spectral data: amount of CIP solubilized, partition coefficient (*P*), and standard free energy of solubilization (Δ*G*) in 12Cho.Br and CTAB systems in absence and presence of 0.3%Ac at 298.15K.

Table S6. Showing Aggregation number *(N_{Agg})*, number of molecules solubilized *(n_s)*, number of micelles available (n_m)

Table S7. Physiochemical descriptors of various systems based on DFT calculations.

Table S1. DIFT parameters for (4mM) 12Cho.Br with different concentration of CIP at 298.15K.

Conc(mM)	γ_m *(mNm^{-1})*	$D_{t\to o}$*(m^{2}s^{-1})*	$D_{t\to\infty}$*(m^{2}s^{-1})*	n	t*(s)
12Cho.Br-CIP					
0.1	34.28	14.32×10^{2}	227.07×10^{-1}	0.680	33.19
0.2	33.25	37.96×10^{-2}	51.93×10^{-1}	0.658	29.76
0.4	33.28	97.48×10^{-3}	12.22×10^{-1}	0.626	21.61
0.6	32.81	46.99×10^{-3}	53.60×10^{-2}	0.652	16.98
0.8	32.08	27.63×10^{-3}	28.04×10^{-2}	0.627	14.36
1.0	31.24	19.81×10^{-3}	17.22×10^{-2}	0.639	10.38
1.2	31.29	14.04×10^{-3}	11.38×10^{-2}	0.577	5.46
1.6	31.49	78.69×10^{-4}	64.67×10^{-3}	0.686	7.37
2.0	30.69	51.90×10^{-4}	41.79×10^{-3}	0.672	8.84

Table S2. DIFT parameters for (4mM) 12Cho.Br(0.3%Ac) with different concentration of CIP at 298.15K.

Conc(mM)CIP	γ_m *(mNm^{-1})*	$D_{t\to o}$*(m^{2}s^{-1})*	$D_{t\to\infty}$*(m^{2}s^{-1})*	n	t*(s)
12Cho.Br-CIP-0.3%Ac					
1.0	30.29	19.53×10^{-3}	12.85×10^{-2}	0.659	42.31
2.0	29.17	50.75×10^{-4}	31.80×10^{-3}	0.670	46.97
4.0	28.74	13.33×10^{-4}	74.81×10^{-4}	0.693	43.72
6.0	27.94	60.30×10^{-5}	32.35×10^{-4}	0.694	45.21
9.0	27.35	27.83×10^{-5}	13.77×10^{-4}	0.649	37.16
11.0	27.93	19.98×10^{-5}	88.16×10^{-5}	0.606	17.33
13.0	27.83	14.45×10^{-5}	63.44×10^{-5}	0.634	20.00
14.0	28.51	12.70×10^{-5}	54.19×10^{-5}	0.665	15.35
16.0	28.17	99.67×10^{-6}	41.51×10^{-5}	0.695	16.38

Table S3. DIFT parameters for (0.5mM) Ctab with different concentration of CIP at 298.15K.

Conc(mM)CIP	γ_m *(mNm^{-1})*	$D_{t\to o}$*(m^{2}s^{-1})*	$D_{t\to\infty}$*(m^{2}s^{-1})*	n	t*(s)
CTAB-CIP					
0.10	35.88	15.66×10^{-1}	120.42×10^{-1}	0.606	21.32
0.14	34.85	83.62×10^{-2}	58.09×10^{-1}	0.626	25.28
0.18	34.06	53.39×10^{-2}	32.35×10^{-1}	0.582	18.07
0.22	33.38	37.16×10^{-2}	20.74×10^{-1}	0.626	21.83
0.26	33.02	27.54×10^{-2}	15.15×10^{-1}	0.627	20.80
0.32	33.24	19.24×10^{-2}	93.35×10^{-2}	0.602	10.28
0.40	33.21	12.36×10^{-2}	57.70×10^{-2}	0.635	11.47
0.50	33.95	80.82×10^{-3}	36.86×10^{-2}	0.581	4.83
0.60	33.56	57.16×10^{-3}	25.20×10^{-2}	0.637	6.42

Table S4. DIFT parameters for (0.5mM) CTAB (0.3%Ac) with different concentration of CIP at 298.15K.

Conc(mM)CIP	γ_m (mNm^{-1})	$D_{t\to o}(m^2s^{-1})$	$D_{t\to\infty}(m^2s^{-1})$	n	t*(s)
CTAB-CIP-0.3%Ac					
1.0	33.05	20.92×10^{-3}	92.45×10^{-3}	0.614	5.86
2.0	32.56	54.82×10^{-4}	21.93×10^{-3}	0.669	5.48
3.0	31.91	25.06×10^{-4}	91.33×10^{-4}	0.560	3.58
5.0	31.53	93.29×10^{-5}	31.79×10^{-4}	0.528	2.44
7.0	31.32	49.13×10^{-5}	15.21×10^{-4}	0.585	2.06
9.0	30.86	30.51×10^{-5}	89.56×10^{-5}	0.671	2.51
11.0	30.39	20.79×10^{-5}	57.87×10^{-5}	0.578	1.75
13.0	30.07	15.13×10^{-5}	42.04×10^{-5}	0.526	1.44
14.0	30.11	13.09×10^{-5}	34.86×10^{-5}	0.501	1.01

Table S5. Showing different parameters calculated from UV-Visible spectral data: amount of CIP solubilized, partition coefficient (*P*), and standard free energy of solubilization (Δ*G*) in 12Cho.Br and CTAB systems in absence and presence of 0.3%Ac at 298.15K.

	12Cho.Br (mM)						
Concentration	**0.1**	**1**	**2**	**4**	**6**	**10**	**15**
CIP Solubility (mM)							
12Cho.Br	0.66	0.70	0.71	1.10	1.30	1.63	1.74
12Cho.Br (0.3%Ac)	7.711	9.40	12.13	12.80	13.32	14.59	15.59
Partition coefficient (*P*)							
`12Cho.Br	10.11	10.80	10.93	17.46	20.76	26.23	28.13
12Cho.Br (0.3%Ac)	127.51	155.68	201.18	212.48	221.01	242.21	258.88
Δ*G* (kJ/mol)							
12Cho.Br	-5.73	-5.89	-5.92	-7.08	-7.51	-8.09	-8.26
12Cho.Br (0.3%Ac)	-12.01	-12.50	-13.14	-13.27	-13.37	-13.60	-13.76
	CTAB (mM)						
Concentration	**0.1**	**0.3**	**0.5**	**0.7**	**0.9**	**1.2**	**1.5**
CIP Solubility (mM)							
CTAB	0.25	0.29	0.31	0.38	0.45	0.49	0.52
CTAB (0.3%Ac)	7.69	8.89	9.51	10.17	10.71	11.04	11.20
Partition coefficient (*P*)							
CTAB	3.20	3.88	4.28	5.43	6.65	7.31	7.71
CTAB (0.3%Ac)	127.21	147.18	157.53	168.500	177.516	183.13	185.70
Δ*G* (kJ/mol)							
CTAB	-2.88	-3.36	-3.60	-4.19	-4.69	-4.93	-5.06
CTAB (0.3%Ac)	-12.01	-12.36	-12.53	-12.70	-12.83	-12.90	-12.94

Table S6. Showing Aggregation number (N_{Agg}), number of molecules solubilized (n_s), number of micelles available (n_m)

System	(N_{Agg})	n_s	n_m
12Cho.Br	41	--	1.38×10^{20}
12Cho.Br-0.3%Ac	48	--	1.08×10^{20}
12Cho.Br-CIP	44	08	1.22×10^{20}
12Cho.Br-CIP-0.3%Ac	41	60	1.45×10^{20}
CTAB	33	--	2.77×10^{19}
CTAB-0.3%Ac	32	--	2.52×10^{19}
CTAB-CIP	26	06	3.29×10^{19}
CTAB-CIP-0.3%Ac	29	195	3.28×10^{19}

Table S7. Physiochemical descriptors of various systems based on DFT calculations.

Parameters	CIP	CTAB	12Cho.Br	CTAB- CIP	12Cho.Br-CIP
E_{LUMO} (-)	0.06089	0.02193	0.02638	0.07467	0.07792
E_{HOMO} (-)	0.20119	0.26503	0.27359	0.21216	0.21059
$E_{LUMO} - E_{HOMO}$	0.14030	0.28696	0.29997	0.13749	0.13267
$E_{HOMO} + E_{LUMO}$ (-)	0.26208	0.2431	0.24721	0.28683	0.28851
Chemical hardness (η)	0.07015	0.14348	0.14998	0.06874	0.06633
Electronegativity (χ)	0.13104	0.12155	0.123605	0.14341	0.14425
Softness (S)	7.12758	3.48480	3.33366	7.27325	7.53749
Chemical potential (μ) (-)	0.13104	0.12155	0.12360	0.14341	0.14425
Global electrophilicity index(ω)	0.12239	0.05148	0.05093	0.14959	0.15685
Dipole moment(Debye)	15.3246	39.5339	22.6555	22.5239	14.0494
E (optimized structure) (-)	1148.567	804.129	761.385	1952.521	1909.776